Clin Physiol & Func Im (2002) **22,** pp361–369

REVIEW ARTICLE

# Elucidation of structure–function relationships in the lung: contributions from hyperpolarized $^3$helium MRI

Hans-Ulrich Kauczor[1] and Balthasar Eberle[2]

*Departments of [1]Radiology, and [2]Anesthesiology, Johannes Gutenberg-University, Mainz, Germany*

## Summary

Magnetic resonance imaging (MRI) using hyperpolarized $^3$helium (He) gas as the source of signal provides new physiological insights into the structure–function relationships of the lung. Traditionally, lung morphology has been visualized by chest radiography and computed tomography, whereas lung function was assessed by using nuclear medicine. As all these techniques rely on ionizing radiation, MRI has some inherent advantages. $^3$He MRI is based on 'optical pumping' of the $^3$He gas which increases the nuclear spin polarization by four to five orders of magnitude translating into a massive gain in signal. Hyperpolarized $^3$He gas is administered as an inhaled 'contrast agent' and allows for selective visualization of airways and airspaces. Straightforward gas density images demonstrate the homogeneity of ventilation with high spatial resolution. In patients with lung diseases $^3$He MRI has shown a high sensitivity to depict ventilation defects. As $^3$He has some more exciting properties, a comprehensive four-step functional imaging protocol has been established. The dynamic distribution of ventilation during continuous breathing can be visualized after inhalation of a single breath of $^3$He gas using magnetic resonance (MR) sequences with high temporal resolution. Diffusion weighted $^3$He MRI provides a new measure for pulmonary microstructure because the degree of restriction of the Brownian motion of the $^3$He atoms reflects lung structure. Since the decay of $^3$He hyperpolarization is dependent on the ambient oxygen concentration, regional and temporal analysis of intrapulmonary $pO_2$ becomes feasible. Thus, pulmonary perfusion, ventilation/perfusion ratio and oxygen uptake can be indirectly assessed. Further research will determine the significance of the functional information with regard to physiology and patient management.

**Correspondence**

*Hans-Ulrich Kauczor, Department of Radiology, Johannes Gutenberg University, Langenbeckstr. 1, DE55131 Mainz, Germany*

*E-mail: kauczor@radiologie.klinik.uni-mainz.de*

**Accepted for publication**

*Received 18 July 2002; accepted 30 August 2002*

**Key words**

*lung; MRI; hyperpolarization; inert noble gases; non-proton MRI; ventilation.*

## Introduction

Traditionally, imaging of the lung consists of morphological visualization of the structure of mediastinum, great vessels, airways and parenchyma, which requires high spatial resolution and high contrast to noise. This is best performed by computed tomography (CT), which is generally regarded as the imaging modality of choice for the morphological assessment of the lung. Maximum spatial resolution is achieved by the use of high resolution CT, i.e. the acquisition of thin single slices with a thickness of 1 mm. Recently, the introduction of multislice CT has led to a paradigm shift because of volume acquisition with almost isotropic voxels. These data sets are extremely well suited for further postprocessing, such as multiplanar reformatting, shaded surface displays and volume rendering. High contrast to noise is given for CT of the lung as air and tissue possess highly different attenuation values. All postprocessing should be aimed at improved and facilitated display of information or extraction of additional information. Ongoing developments also strive to assess aspects of lung function. Dedicated acquisition or postprocessing techniques are necessary for surrogate measurements of functional properties or characteristics of pathology (Kramer & Hoffman, 1995; Ley et al., 2002). Several approaches have been described in the literature. They include the acquisition of scans obtained at full inspiratory and expiratory position. They allow to detect and differentiate air trapping and hypoventilation, which may be associated with expiratory obstruction of small airways and hypoxic vasoconstriction (Kauczor *et al.*, 2000, 2002b). Although images from two different positions within the respiratory cycle are available for evaluation, complete coverage is desirable. This can be achieved by

 

continuous dynamic imaging, so-called dynamic multiscan or cine CT. Thus, images of a single slice with a temporal resolution of 100 ms can be acquired (Markstaller *et al.*, 2001). All these techniques make use of air as the inherent contrast mechanism in CT of the lung. As there is already a residual gas phase present within the aerated lung, and because only its volume changes during the respiratory cycle, it is not trivial to directly visualize its ventilatory exchange and to assess its distribution. This can be carried out by use of an inhaled contrast agent, preferably with higher density than air and administered by inhalation. These prerequisites are met by xenon gas (Simon *et al.*, 1998). Although technically feasible, the method has not gained widespread acceptance. In summary, CT is the gold standard for imaging lung structure. The significance of CT-based surrogate measurements of lung function parameters is still under investigation. Further techniques are required to quantify pathological function and assign it topographically within the lung.

Nuclear medicine is well established for functional investigations of ventilation, perfusion and their regional matching in the lung. Several tracers have been used to visualize the distribution of ventilation, each with its own advantages and disadvantages. Gases, such as xenon or krypton, have the advantage of greater ease of distribution into the smaller airways, whereas aerosols, such as technegas, are easier to handle but are more prone to central deposition (White *et al.*, 1991). For routine applications, results are displayed as planar images. They are limited with regard to spatial and temporal resolution. Single photon emission computed tomography (SPECT) offers improved anatomical detail, but it is associated with a negative effect on temporal resolution (Nagao *et al.*, 2000). In contrast, positron emission tomography (PET) can provide an in-plane resolution of ~5 mm and a temporal resolution in the range of 30 s. However, PET of the lung is not ready for broad clinical use, yet, because the technical requirements, especially dedicated tracers, are not widely available (Schuster, 1998).

In comparison with CT and nuclear medicine, the lack of ionizing radiation is a common driver to introduce magnetic resonance imaging (MRI) to the arena of functional imaging of thoracic disease. As a result of the inherent characteristics, MRI of the lung is inferior to CT with regard to the visualization of pulmonary structure which is based on spatial and contrast resolution. However, there are also a variety of important effects and mechanisms in MRI which allow for functional imaging. These techniques are already established for MRI of the brain and the heart, and they are now applied to the lung, where they enable radiologists to provide new image-based strategies for the functional assessment of ventilation (Kauczor *et al.*, 1998). In comparison with nuclear medicine, MRI has clear advantages with respect to spatial and temporal resolution.

A revolutionary approach was the introduction of hyperpolarized $^3$Helium ($^3$He) gas as a novel contrast mechanism in MRI. The gas is administered by inhalation and leads to a selective display of the ventilated airspaces. As a result of the particular properties of hyperpolarized $^3$He in MRI, additional functional information of ventilation and the airspaces can be derived. The purpose of this paper is to review the recent results of this technique with respect to improved insights into structure and function of the lung.

## Methods

### Preparation of hyperpolarized gas and technical requirements

MRI making use of the hyperpolarization of $^3$He has to operate on a different Larmor frequency than traditional proton MRI. In contrast to most contrast agents used in proton MRI which rely on paramagnetic effects of the compound onto the T1 relaxation of blood or tissue, hyperpolarized $^3$He itself is the source of signal and can be used as an inhaled 'contrast agent'. Helium is in current use in the area of lung function analysis for measurements of the residual volume as well as in pulmonary critical care and anaesthesiology for treatment of exacerbated chronic obstructive pulmonary disease (COPD) and malignant airway obstruction (Rodrigo *et al.*, 2002). Besides, it is widely used in deep sea diving for decompression. From all these applications we know that this inert noble gas is not absorbed in considerable amounts and has no adverse effects. The only difference between these applications and $^3$He MRI is the necessity of using the rare isotope $^3$He instead of $^4$He, which is abundant in the atmosphere. $^3$He is a byproduct of tritium ($^3$hydrogen) decay which explains its declaration as a strategic product in the USA.

Under normal conditions, the spin density of $^3$He gas is too low to be detectable at MRI. Another property of $^3$He helps to make it attractive for MRI. For decades nuclear physicists have used $^3$He for studies aimed at insights of the structure of neutrons. They required hyperpolarized $^3$He for these experiments. Hyperpolarization is achieved by the transfer of photon angular momentum transfer to the nuclei of atoms such as $^3$He. For this purpose, polarized light from high-power lasers is used in a process called optical pumping. Optical pumping can be performed in different ways, notably spin exchange or metastability exchange (Kauczor *et al.*, 1998). They have different profiles with regard to performance, safety and ease of use. There are rather specific requirements for storage and transport because any interaction with paramagnetic or ferromagnetic substances, such as oxygen or iron, or magnetic stray fields will irreversibly destroy the non-equilibrium polarization. Such requirements can be met by dedicated glass cells together with a magnetic-holding field. Once met, the hyperpolarization necessary for imaging studies can be kept for at least 72 h (Heil *et al.*, 1995). Ground and air transport of laser-polarized $^3$He is thus feasible (Wild *et al.*, 2002).

### $^3$He Delivery to the patient

Gas dosage and administration are accomplished either by inhalation from prefilled collapsible bags or by using a dedicated

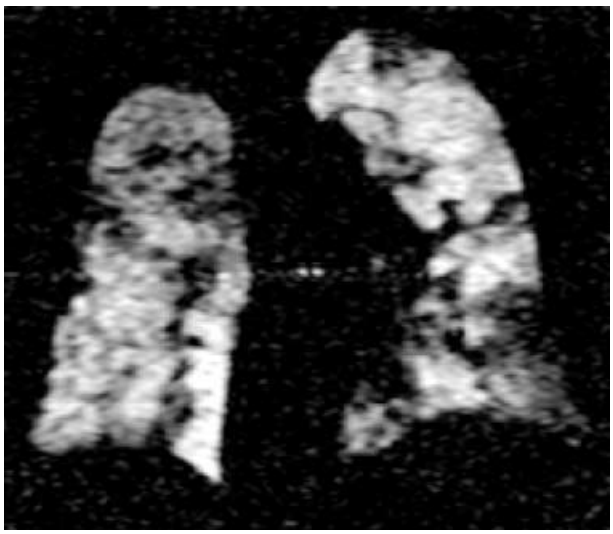

**Figure 1** A 72-year-old male patient with chronic bronchitis without emphysema. Gas density image shows segmental areas of hypoventilation.

PC-controlled applicator device (international patent PCT/EP/98/07516). The $^3$He bag is filled with up to 1 l of either pure $^3$He or with a mixture of polarized $^3$He with medical nitrogen, and the total content of the bag is inhaled followed by breath-holding and image acquisition. The applicator device, on the other hand, allows insertion of bolus amounts (between 20 and 500 ml) of $^3$He into any phase of the inspiratory cycle, followed by the normal respiratory gas mixture. To this end, the applicator is connected into the inspiratory limb of a valved one-way breathing circuit. It allows to administer the tracer gas during spontaneous breathing or, if connected to an intensive care-type respirator machine, also during a variety of assisted or controlled ventilation modes (Fig. 1). Thus, a typical $^3$He dose of 200–300 ml is inhaled within a single inspiration through a nasal continuous positive airway pressure (CPAP) mask or via a mouthpiece at the beginning of an inspiration. The bolus is chased by room or oxygen-enriched air as required by the patient. Throughout the procedure, heart rate and oxygenation of the patient are monitored by finger pulse oximetry. Also, respiratory flows, volume and gas concentrations can be measured and recorded. Supplemental $O_2$, inspiratory pressure support or CPAP can be provided for patients with significantly impaired lung function. Duration of a typical study is presently 40 min.

## Results

Since the first studies in humans in 1995 (Ebert *et al.*, 1996) a lot of expertise has been accumulated. Besides the mere detection of the hyperpolarized $^3$He gas within the lung after inhalation, more sophisticated MR sequences have been developed and applied in volunteers and patients (de Lange *et al.*, 1999; Kauczor *et al.*, 2001a, 2002a; Moeller *et al.*, 2002). Based on these encouraging reports, four principal steps have been established to form a functional imaging protocol. It provides information on static and dynamic distribution of ventilation, on pulmonary microstructure and oxygen partial pressure within ventilated airspaces.

Gas density $^3$He MRI is performed to obtain a highly resolved slice-selective set of images covering the entire lung. The acquisition is typically performed during a breath-hold of approximately 10 s after inhalation of the hyperpolarized $^3$He gas. Signal-to-noise ratio (SNR) is to be high and homogeneous throughout the lung. The images are a static snapshot of the distribution of ventilation during this single-breath manoeuvre. Regions which the gas bolus has already passed – e.g. the trachea, or where the gas has not yet entered, such as areas with long inspiratory time constants – because of inspiratory airway obstruction, are not visualized and appear therefore as signal voids. As known from nuclear medicine, a normally ventilated lung is represented by an almost homogeneous distribution of the hyperpolarized $^3$He gas (Kauczor *et al.*, 1998). In supine position only very few and small (diameter <1 cm) gravity-dependent voids or ventilation defects are appreciated in the periphery of the lung (Mata *et al.*, 1998). Such small and transient ventilation defects are not considered as pathological findings, because occasional air-trapping of secondary lobules is regularly detected in normal lungs at CT performed in full expiratory position. A larger number of ventilation defects, however, is observed in smokers with normal pulmonary function tests (PFTs) in comparison with non-smokers with normal pulmonary function tests (Guenther *et al.*, 2000). This indicates the high sensitivity of $^3$He MRI in the identification of regional ventilatory impairment, when compared with routine PFTs. In lung disease, numerous regional ventilation defects are a common finding. Such defects have been described in a large variety of different pulmonary disorders such as COPD with and without emphysema (Kauczor *et al.*, 1997; de Lange *et al.*, 1999), bronchiectasis (Donnelly *et al.*, 1999), asthma (Altes *et al.*, 2001), bronchiolitis obliterans following lung transplantation (McAdams *et al.* 1999; Gast *et al.*, 2002b), fibrosis or tumours (Kauczor *et al.*, 1998) (Figs 1–4). Unfortunately, neither the morphological appearance of these ventilation defects nor their pattern is very helpful in differential diagnosis. Thus, here is a definite lack of specificity, and further studies are warranted to elucidate the causes of ventilation defects and their localization in different diseases (Figs 1–4). This low degree of specificity is associated with a very high sensitivity, much higher than CT, nuclear medicine or PFTs (Gast *et al.*, 2002b). In a comparative study, plausible correlates were detected at CT for only 63% of ventilation defects seen at $^3$He MRI (Gast *et al.*, 2002b).

Furthermore, gas density $^3$He MRI can also be used to calculate the volume of ventilated airspace in the lungs. From the data sets, threshold-based segmentations are performed, and the volumes are integrated. The resultant volumetry shows good correlation with results from PFTs ($r = 0{\cdot}9$) in healthy volunteers (Kauczor *et al.*, 2001b ), with systematic offsets caused by supine (MRI) vs. sitting (PFT) posture, as well as because of contributions from tissue and blood volume con-

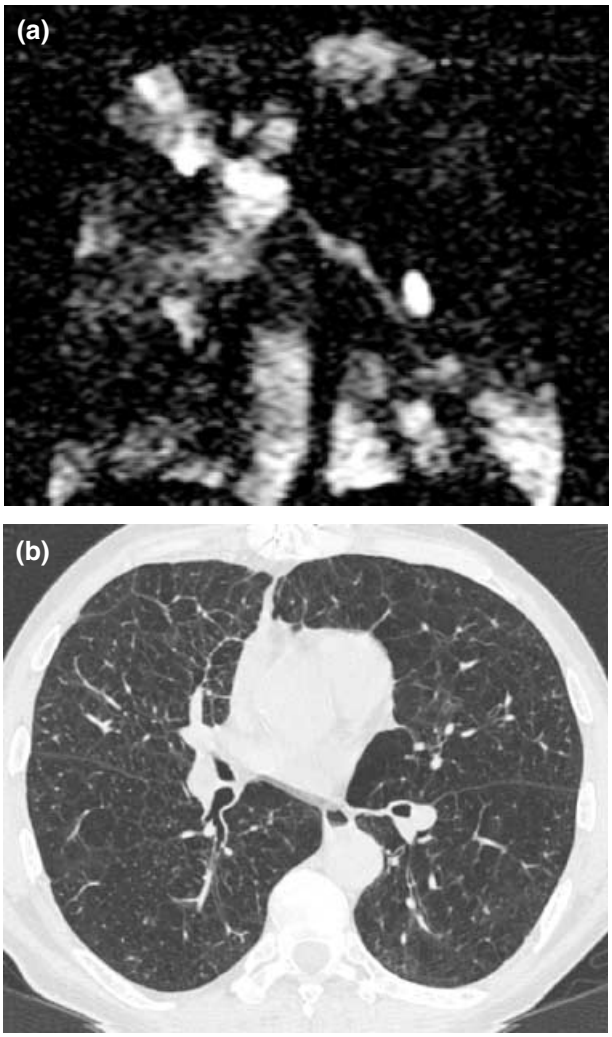


**Figure 2** A 57-year-old male patient with severe emphysema. (a) Gas density image shows multiple widespread ventilation defects throughout both lungs; (b) corresponding CT shows emphysematous destruction in both lungs.

**Figure 3** A 35-year-old male patient shortly after double lung transplantation with chronic rejection and re-transplantation on the left. Gas density image shows normal ventilation of the recent graft on the left and almost complete lack of ventilation on the right with filling of the central airways indicative for bronchiolitis obliterans.

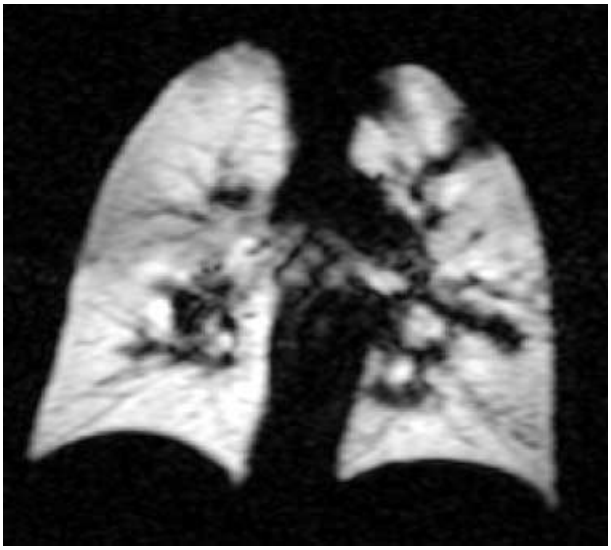

**Figure 4** A 33-year-old male patient with chronic thrombo-embolic pulmonary hypertension. Gas density image shows minor wedge-shaped ventilation defects representing concomitant airway disease most likely because of smoking.

tained within the segmented volume. In patients, the correlation was also good ($r = 0{\cdot}96$), although absolute volume measurements differed more than in healthy subjects (Markstaller *et al.*, 2002).

Dynamic imaging $^3$He MRI is based on the use of sequences with high temporal resolution in a range of 30–130 ms per image. Different MR techniques are available to meet these requirements, such as an ultrafast FLASH sequence (Schreiber *et al.*, 2000) echo planar imaging (Saam *et al.*, 1999) or spiral imaging (Salerno *et al.*, 2001). Dynamic image series illustrate the distribution of a single breath of $^3$He gas throughout the entire breathing cycle (Fig. 5). In normal subjects, a very fast inflow through the central airways followed by synchronous distribution into the peripheral airspaces and then homogeneous filling of the alveolar space is observed (Schreiber *et al.*, 2000). In patients, irregular and asynchronous distribution patterns with sequential filling of peripheral airspaces, redistribution during re-breathing and air trapping have been described (Gierada *et al.*, 2000). In single lung transplant recipients with fibrosis or emphysema as the underlying disease, who offer a model of two functionally very different lungs, $^3$He MRI nicely demonstrates preferential ventilation of the well-functioning graft (Gast *et al.*, 2002a). Beyond the mere visual impression of asynchronous and inhomogeneous distribution of ventilation,

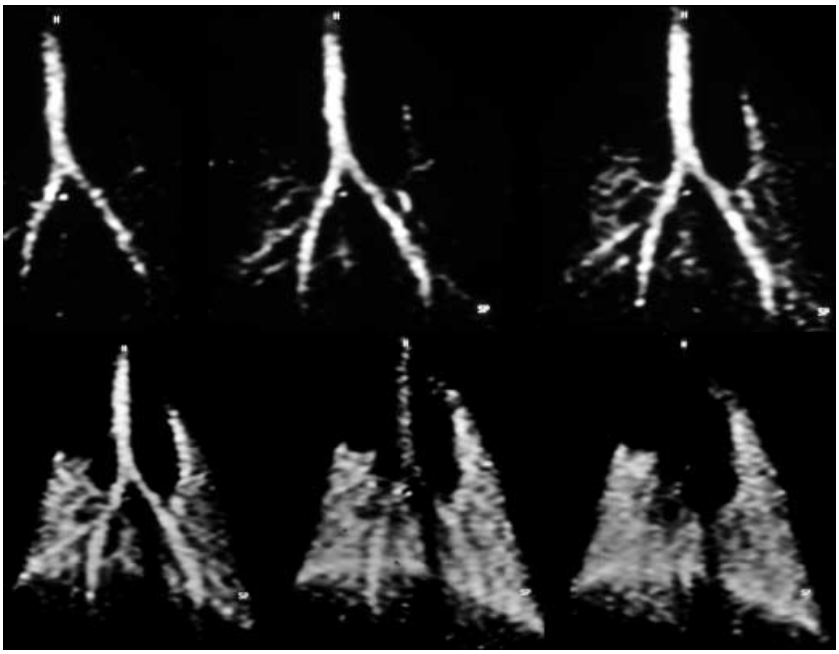

**Figure 5** Dynamic ventilation $^{3}$He-MRI after inhalation of hyperpolarized He-3 gas in an animal experiment (pig) shows a rapid and homogeneous filling of the airspaces bilaterally.

quantitative parameters can be derived from the image series, e.g. the tracheal transit time of the inhaled $^{3}$He bolus, a tracheo-alveolar time interval until the signal arrives in the periphery, the alveolar rise time of the signal curve and the alveolar signal amplitude (Gast *et al.*, 2002a). However, because of the tidal nature of ventilation, a problem arises which is not as prominent, for instance, in solid organ perfusion studies. A simple evaluation based on spatially fixed regions of interests (ROIs) appears unsatisfactory in the lung because it expands and shrinks considerably during the respiratory cycle, and different lung regions would be measured each time within a fixed voxel. To account at least for the apico-basal cycling of the dynamic lung images, a motion correction algorithm based on a linear transformation was developed. It normalizes all images of a dynamic series to a mid-inspiratory level of expansion and thus improves the topographical validity of the ROI-based measurements (Gast *et al.*, 2002a). In single lung transplant recipients, inspiratory gas inflow to the graft was found to start earlier and to last longer than that to the native diseased lung (Gast *et al.*, 2002a).

Diffusion-weighted $^{3}$He MRI is a dedicated MRI technique to measure the random microscopic molecular movement (Brownian motion). The term diffusion is therefore not to be confused with other types of diffusional gas movement in the lung such as (1) alveolocapillary gas exchange which is assessed by measuring diffusion capacity of carbon monoxide, or (2) diffusive gas transport within the peripheral airways following a concentration gradient, which is the counterpart to convective gas transport in the large airways.

In contrast, Brownian motion of $^{3}$He atoms measured by MRI relates to their random motion irrespective of a concentration gradient. To this purpose special pulse sequences known from proton MRI are used. During an inspiratory breath-hold after inhalation of the hyperpolarized $^{3}$He gas, bipolar gradients are applied prior to signal acquisition to dephase and rephase spins (Moeller *et al.*, 2002). All those spins that have diffused away from their original position will contribute to signal attenuation; hence the images will be weighted for diffusion. As $^{3}$He atoms are very small they are highly diffusible (diffusion constant $\sim$2 cm$^{2}$ s$^{-1}$). The luminal dimensions of bronchioles and alveoli represent a major restriction to the diffusive motion of the $^{3}$He atoms. This restriction can be measured by diffusion-weighted MRI and is calculated as the apparent diffusion coefficient (ADC). Normal pulmonary parenchyma is characterized by rather low ADC values in the range between 0·17 and 0·28 cm$^{2}$ s$^{-1}$ (Mugler *et al.*, 1998; Hanisch *et al.*, 2000a; Saam *et al.*, 2000; Salerno *et al.*, 2000a). Histogram analysis shows a homogeneous and narrow distribution with a single peak. In supine position, gravity exerts some influence on the distribution of the ADC values, which exhibit an antero-posterior gradient with lower ADC values in dorsal lung areas on expiration (Bink *et al.*, 2001) and which diminishes on inspiration (Salerno *et al.*, 2000b). This observation parallels attenuation measurements at CT (Kauczor *et al.*, 2000) with the antero-posterior gradient being quite marked on scans obtained at full expiration and small or absent on scans obtained at full inspiration (Verschakelen *et al.*, 1993). Increased ADC values reflect an increase in the size of peripheral airways and alveoli. The most prevalent example is emphysema which is defined as the constant and irreversible abnormal enlargement of the alveoli distal to the terminal bronchioles (Snider *et al.*, 1985). In both animal experiments with induced emphysema as well as in investigations in emphysema patients, the increase in alveolar size was associated with higher ADC values (Fig. 6). According to the extent and severity of disease, ADC values vary between 0·4 and 0·9 cm$^{2}$ s$^{-1}$ (Saam *et al.*, 2000; Chen *et al.*, 2000;

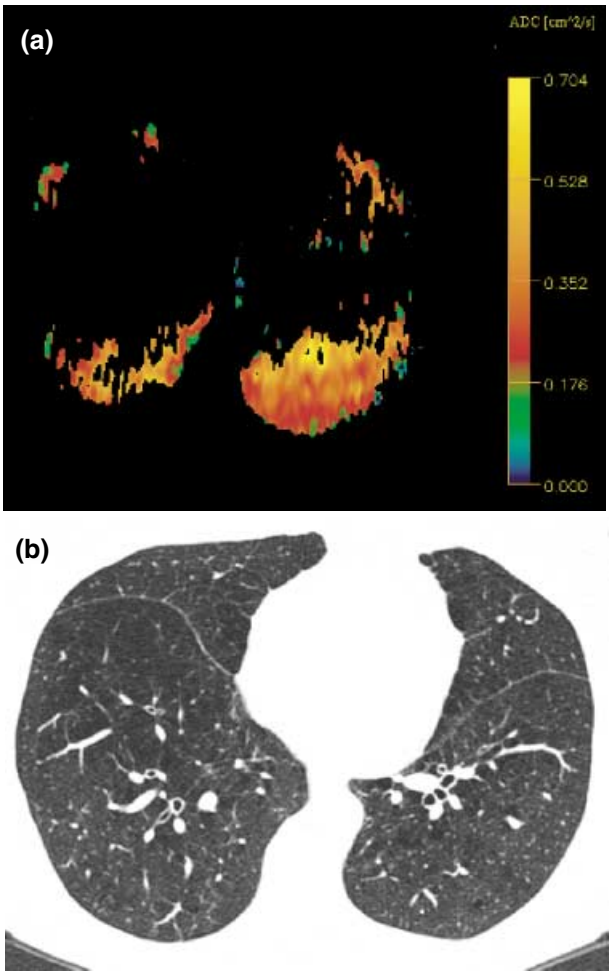


**Figure 6** A 63-year-old female patient with emphysema. (a) The colour-coded map of the apparent diffusion coefficient (ADC) shows increased values with a mean of 0·35 $cm^2$ s−1. ADC values cannot be determined within large ventilation defects. (b) Corresponding CT also shows widespread emphysema.

Hanisch *et al.*, 2000a). Histogram analysis reveals broadening of the distribution and reduction of the peak height, representing parenchymal destruction and inhomogeneous distribution of the disease process (Mugler *et al.*, 1998; Salerno *et al.*, 2002). The spatial distribution of the areas with highest ADC values reflects the well-known apical predominance of centrilobular emphysema (Salerno *et al.*, 2002). The antero-posterior ADC gradient is lost (Bink *et al.*, 2001). As emphysema is associated with bronchial obstruction as measured by forced expiratory volume in 1 s (FEV1), ADC values have been shown to correlate closely with FEV1 ($r = 0{\cdot}8$) (Salerno *et al.*, 2002). End-stage lung in fibrosis is also associated with an increase in peripheral airspace dimensions, such as within traction bronchiectasis and honeycomb cysts. Consequently, increased ADC values with a mean of 0·35 $cm^2$ $s^{-1}$ are observed (Hanisch *et al.*, 2000a). In a control group of healthy subjects, these same authors found that gas diffusion in the alveolar space and the peripheral airways was almost isotropic. In diseased lungs, however, diffusive motion appears anisotropic (Hanisch *et al.*, 2000b; Yablonskiy *et al.*, 2002). Anisotropy of diffusive gas motion may, for instance, indicate non-spherical geometrical changes which may give diffusive gas motion a preferential direction. All these data indicate that diffusion-weighted $^3$He MRI may serve as a novel, non-invasive tool to quantitate pulmonary microstructure without the burden of ionizing radiation.

Oxygen-sensitive $^3$He MRI is based upon the destructive effect of paramagnetic molecules towards the non-equilibrium ('hyper') polarization of optically pumped $^3$He. In somewhat simplified terms, the most abundant paramagnetic molecule in inspired and alveolar gas, which is $O_2$, reduces magnetization and hence, signal intensity of inhaled hyperpolarized $^3$He rapidly – i.e. within a breath-hold's time – to its nearly unmagnetized normal state. The rate of signal decay R (t) depends on the ambient partial pressure of oxygen ($PO_2$), according to the proportional relationship $R(t) = PO_2 / \xi$, with a so-called relaxation time constant $\xi = 2{\cdot}61$ s bar (Saam *et al.*, 1995). At first, this interaction of polarization with alveolar $O_2$ had been considered a nuisance, when researchers focused primarily on 'nice' gas density images of the lung. Soon it was realised, however, that this $O_2$ sensitivity of $^3$He polarization could make the gas an indicator substance for the measurement of instantaneous and regional intra-alveolar $PO_2$ (Eberle *et al.*, 1999). The latter is a physiologically interesting variable because it is uniquely dependent on the ventilation–perfusion ratio prevailing in the region imaged.

In practical terms, the kinetics of signal decay are obtained from serial FLASH images acquired during one or two breath-holds. The contribution of the $PO_2$ effect to the total signal decay rate is isolated from that of the imaging process, which in itself also destroys magnetization, and is quantified. Several techniques have been described to determine regional $PO_2$ at the very beginning of a breath-hold manoeuvre as well as the rate of its decrease during breath-holding (Eberle *et al.*, 1999; Deninger *et al.*, 1999, 2000). This rate of decrease is the net result of both alveolocapillary $O_2$ transfer and non-ventilatory mass movement of fresh gas to replace it.

Image-based determination of intrapulmonary $PO_2$ has been validated in phantom experiments, in animals and human volunteers exposed to various inspired $O_2$ concentrations (Eberle *et al.*, 1999; Deninger *et al.*, 2000, 2002). In confirmation with these findings, other researchers have also related relaxation kinetics to intrapulmonary $PO_2$ in small animals *in vivo* and postmortem, and have obtained plausible estimates of oxygen uptake from the lungs and cardiac output from this information (Moeller *et al.*, 2001). In healthy human subjects, a very homogeneous $PO_2$ distribution has been described with this technique, its mean being in good agreement with end-tidal $PO_2$ measured at the mouth (Fig. 7). However, in patients with pulmonary fibrosis after unilateral lung transplantation, image-based alveolar $PO_2$ was found to be heterogeneously distributed, i.e. it was higher in functioning grafts than in native fibrotic lungs. Mean MRI-determined alveolar $PO_2$ of these patients ranged quite consistently between $PO_2$ levels determined in end-tidal gas and arterialised blood (Eberle *et al.*, 2000). More recent

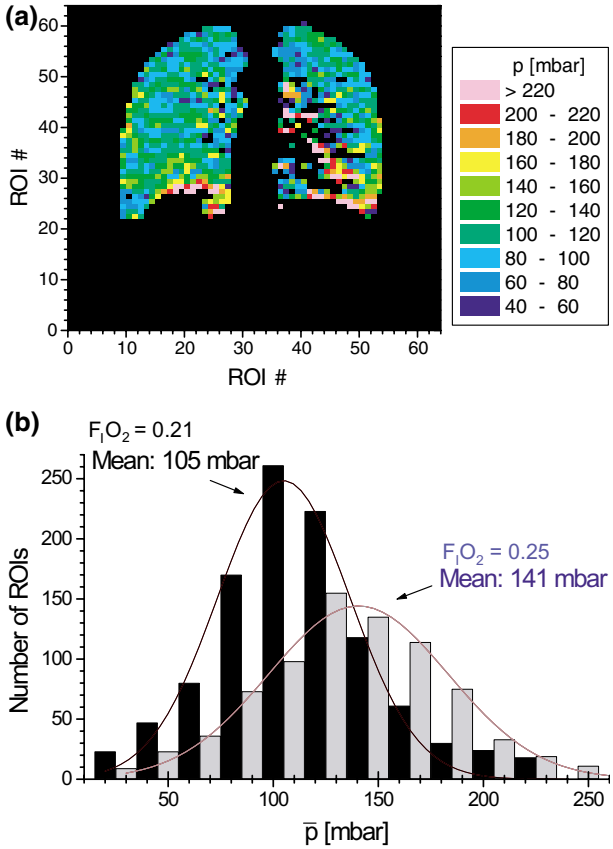


**Figure 7** (a) Map of intrapulmonary $PO_2$ at the beginning of breathhold () after inhalation of 250 ml of $^3$He. Colour-coded data are derived from serial $^3$He projection imaging in a healthy subject breathing normal room air ($F_I O_2 = 0{\cdot}21$). (b) Histograms of intrapulmonary $PO_2$ distributions in another healthy subject inhaling either normal room air ($F_I O_2 = 0{\cdot}21$, dark columns) or oxygen-enriched air ($F_I O_2 = 0{\cdot}25$, light columns) together with 250 ml hyperpolarised $^3$He (from Deninger AJ *et al.*, Magn Reson Med 47: 105–114 (2002), with permission). In response to oxygen enrichment by approximately 4 %, the mean of the distribution increases by 36 mbar.

work of the same group demonstrates that alveolar deadspace generated by pulmonary arterial obstruction is topographically correctly detected by MRI-determined alveolar $PO_2$ measurement (Eberle *et al.*, 2002). Meanwhile, intrapulmonary $PO_2$ measurements in small animals have also been shown to be feasible using low-field MRI (Olsson *et al.*, 2002).

Thus, in the future, oxygen-sensitive $^3$He MRI may develop into a quick, non-invasive and easily repeatable method to assess ventilation–perfusion matching, and to estimate oxygen uptake from the lung.

### Conclusion and clinical perspectives

Hyperpolarized $^3$He MRI of the lung is a novel approach to image airways and the alveolar space with high spatial and unmatched temporal resolution. Meanwhile, gas density imaging allows to outline ventilated intrapulmonary airspace, with a resolution to the eighth bronchial generation, and to identify even minute areas of hypoventilation. Dynamic imaging of respiratory cycling casts a new look upon instantaneous distribution of ventilation between and within lungs. Pulmonary microstructure in emphysema and other destructive lung diseases may be assessed by diffusion-weighted $^3$He MRI. $PO_2$-sensitive $^3$He-MRI provides an image-based estimation of regional alveolar $PO_2$ and $O_2$ uptake into the blood.

Efficacy and safety of $^3$He-MRI are currently researched at the level of phase II trials. Potential clinical applications may develop in early detection and therapeutic monitoring of obstructive lung disease; in pre- and postoperative regional lung function analysis for pulmonary resections and lung transplantation; and in early detection and follow-up of bronchiolitis obliterans in lung grafts. General advantages of $^3$He-MRI are the avoidance of radiation exposure, the biochemical inertness of $^3$He and the repeatability of studies, which is limited, at present, mainly by the availability of hyperpolarized $^3$He gas.

## Acknowledgment

The Mainz Helium Project is run by an interdisciplinary group with scientists from the departments of radiology, anaesthesiology, pneumology, thoracic surgery and physics. It is supported by the German Research Council (DFG), European Commission ('COPHIT', 'PHIL'), Max-Planck Society, Alexander von Humboldt Foundation, DAAD, and Amersham Health.

## References

Altes T, Powers P, Knight-Scott J *et al.* Hyperpolarized $^3$He MR lung ventilation imaging in asthmatics: preliminary findings. *J Magn Reson Imag* (2001); **13**: 378–384.

Bink A, Gast K, Hanisch G *et al.* Analysis of airspace size in healthy volunteers and single lung transplant recipients using the apparent diffusion coefficient at $^3$He-MRI. *Eur Radiol* (2001); **11**: S214.

Chen X, Hedlund L, Moeller H, Chawla M, Maronpot R, Johnson G. Detection of emphysema in rat lungs using magnetic resonance measurements of $^3$He diffusion. *Proc Natl Acad Sci* (2000); **97**: 11478–11481.

Deninger A, Eberle B, Ebert M *et al.* Quantitation of regional intrapulmonary oxygen partial pressure evaluation during apnoe by $^3$He-MRI. JMR (1999); **141**: 207–216.

Deninger A, Eberle B, Ebert M *et al.* $^3$He-MRI-based measurements of intrapulmonary $pO_2$ and its time course during apnea in healthy volunteers: first results, reproducibility and technical limitations. *NMR Biomed* (2000); **13**: 194–201.

Deninger A, Eberle B, Bermuth J *et al.* Assessment of a single-acquisition imaging sequence for oxygen-sensitive $^3$He MRI. *Magn Reson Med* (2002); **47**: 105–114.

Donnelly LF, MacFall JR, McAdams HP *et al.* Cystic fibrosis: combined hyperpolarized $^3$He-enhanced and conventional proton MR imaging in the lung-preliminary observations. *Radiology* (1999); **212**: 885–889.

Eberle B, Weiler N, Markstaller K *et al.* Analysis of regional intrapulmonary O2-concentrations by MR imaging of inhaled hyperpolarized helium-3. *J Appl Physiol* (1999); **87**: 2043–2052.

Eberle B, Markstaller K, Lill J *et al.* Oxygen-sensitive $^3$He magnetic resonance imaging of the lungs in patients after unilateral lung transplantation. *Am J Resp Crit Care Med* (2000); **161**: A718.

Eberle B, Markstaller K, Stepniak A, Viallon M, Kauczor H-U. $^3$Helium-MRI-Based Assessment of regional gas exchange impairment during experimental pulmonary artery occlusion. *Anesthesiology* (2002); **96**: A1309.

Ebert M, Großmann T, Heil W *et al*. Nuclear magnetic resonance imaging on humans using hyperpolarized $^3$He. *Lancet* (1996); **347**: 1297–1299.

Gast K, Puderbach M, Rodriguez I *et al*. Dynamic ventilation $^3$He MRI with lung motion correction: gas flow distribution analysis. *Invest Radiol* (2002a); **37**: 126–134.

Gast K, Viallon M, Eberle B *et al*. MR Imaging in lung transplant recipients using hyperpolarized $^3$He: comparison with CT. *J Magn Reson Imag* (2002b); **15**: 268–274.

Gierada D, Saam B, Yablonskiy D, Cooper J, Lefrak S, Conradi M. Dynamic echo planar MR imaging of lung ventilation with hyperpolarized He-3 in normal subjects and patients with severe emphysema. *NMR Biomed* (2000); **13**: 176–181.

Guenther D, Eberle B, Hast J *et al*. $^3$He MRI in healthy volunteers: preliminary correlation with smoking history and lung volumes. *NMR Biomed* (2000); **13**: 182–189.

Hanisch G, Schreiber W, Diergarten T *et al*. Investigation of intrapulmonary diffusion by $^3$He MRI. *Eur Radiol* (2000a); **10**: S345.

Hanisch G, Schreiber W, Kauczor H-U *et al*. Determination of diffusion ansiotropy in the lung by Helium-3 MRI. *Eur Radiol* (2000b); **10**: G3.

Heil W, Humblot H, Otten E, Schäfer M, Surkau R, Leduc M. Very long nuclear relaxation times of spin polarized helium3 in metal coated cells. *Physics Letters A* (1995); **201**: 337–343.

Kauczor H-U, Ebert M, Kreitner K-F *et al*. Imaging of the lungs using $^3$He MRI: preliminary clinical experience. *J Magn Reson Imag* (1997); **7**: 538–543.

Kauczor H-U, Surkau R, Roberts T. MRI using hyperpolarized noble gases. *Eur Radiol* (1998); **8**: 820–827.

Kauczor H-U, Hast J, Heussel C, Schlegel J, Mildenberger P, Thelen M. Focal airtrapping at expiratory high-resolution CT: comparison with pulmonary function tests. *Eur Radiol* (2000); **10**: 1539–1546.

Kauczor H-U, Chen X, van Beek E, Schreiber W. Pulmonary ventilation imaged by magnetic resonance: at the doorstep of clinical application. *Eur Respir J* (2001a); **17**: 1–16.

Kauczor H-U, Markstaller K, Puderbach M *et al*. Volumetry of ventilated airspaces using $^3$He MRI: preliminary results. *Invest Radiol* (2001b); **36**: 110–114.

Kauczor H-U, Hanke A, van Beek E. Assessment of lung ventilation by MR imaging: current status and future perspectives. *Eur Radiol* (2002a); **12**: 1962–1970.

Kauczor H-U, Hast J, Heussel C, Schlegel J, Mildenberger P, Thelen M. Densitometry of paired inspiratory/expiratory high resolution CT comparison with pulmonary function tests. *Eur Radiol* (2002b); DOI 10.1007/s00330-002-1514z.

Kramer SS, Hoffman EA. Physiologic imaging of the lung with volumetric high-resolution CT. *J Thorac Imag* (1995); **10**: 280–290.

de Lange E, Mugler J, Brookeman J *et al*. Lung air spaces: MR imaging evaluation with hyperpolarized He gas. *Radiology* (1999); **210**: 851–857.

Ley S, Mayer D, Brook B *et al*. Radiological imaging as the basis for a simulation software of ventilation in the tracheo-bronchial tree. *Eur Radiol* (2002); **12**: 2218–2228.

Markstaller K, Arnold M, Döbrich M *et al*. A software tool for automatic image-based ventilation analysis using dynamic chest CT-scanning in healthy and ARDS lungs. *Fortschr Röntgenstr* (2001); **173**: 830–835.

Markstaller K, Kauczor H-U, Puderbach M *et al*. $^3$He MRI-based versus conventional determination of lung volumes in patients after unilateral lung transplantation: a new approach to regional spirometry. *Acta Scand Anesth* (2002); **46**: 845–852.

Mata J, Altes T, Christopher J, Mugler J, Brookeman J, deLange E. Transient, position-dependent ventilation defects of the lung in healthy volunteers: demonstration with hyperpolarized helium-3 MR imaging. *Proc Intl Soc Mag Reson Med* (2002); **10**: 2027.

McAdams H, Palmer SM, Donnelly L, Charles H, Tapson V, MacFall J. Hyperpolarized $^3$He-enhanced MR imaging of lung transplant recipients: preliminary results. *AJR* (1999); **173**: 955–959.

Moeller H, Hedlund L, Chen X *et al*. Measurements of hyperpolarized gas properties in the lung. Part III: $^3$He T1. *Magn Reson Med* (2001); **45**: 421–430.

Moeller H, Chen X, Saam B *et al*. MRI of the lungs using hyperpolarized noble gases. *Magn Reson Med* (2002); **47**: 1029–1051.

Mugler J, Brookeman J, Knight-Scott J, Maier T, deLange E, Bogorad P. Regional measurement of the $^3$He diffusion coefficient in the human lung. *Proc Intl Soc Mag Med* (1998); **6**: 1906.

Nagao M, Murase K, Ichiki T, Sakai S, Yasuhara Y, Ikezoe J. Quantitative analysis of technegas SPECT: evaluation of regional severity of emphysema. *J Nucl Med* (2000); **41**: 590–595.

Olsson L, Magnusson P, Deninger A *et al*. Intrapulmonary $pO_2$ measured by low field MR imaging of hyperpolarized $^3$He. *Proc Intl Soc Mag Reson Med* (2002); **10**: 2021.

Rodrigo G, Pollack C, Rodrigo C, Rowe B. Heliox for treatment of exacerbations of chronic obstructive pulmonary disease (Cochrane Review). *Cochrane Database Syst Rev* (2002); **2**: CD003571.

Saam B, Happer W, Middleton H. Nuclear relaxation of $^3$He in the presence of O2. *Phys Rev A* (1995); **52**: 862–865.

Saam B, Yablonskiy DA, Gierada DS, Conradi MS. Rapid imaging of hyperpolarized gas using EPI. *Magn Reson Med* (1999); **42**: 507–514.

Saam B, Yablonskiy D, Kodibagkar V *et al*. MR imaging of diffusion of $^3$He gas in healthy and diseased lungs. *Magn Reson Med* (2000); **44**: 174–179.

Salerno M, Brookeman J, deLange E, Knight-Scott J, Mugler J. Detection of Regional microstructural changes of the lung in emphysema using hyperpolarized 3 He diffusion MRI. *Proc Intl Soc Mag Reson Med* (2000a); **8**: 9.

Salerno M, Brookeman J, Lange Ed, Knight-Scott J, III JM. Demonstration of an alveolar-size gradient in the healthy human lung: a study of the reproducibility of hyperpolarized 3 He diffusion MRI. *Proc Intl Soc Mag Reson Med* (2000b); **8**: 2195.

Salerno M, Altes T, Brookeman J, deLange E, Mugler J. Dynamic spiral MRI of pulmonary gas flow using hyperpolarized $^3$He: preliminary studies in healthy and diseased lungs. *Magn Reson Med* (2001); **46**: 667–677.

Salerno M, Lange Ed, Altes T, Truwit J, Brookeman J, Mugler J. Emphysema: hyperpolarized Helium3 diffusion MR imaging of the lungs compared with spirometric indexes – initial experience. *Radiology* (2002); **222**: 252–260.

Schreiber W, Weiler N, Kauczor H-U *et al*. Ultraschnelle MRT der Lungenventilation mittels hochpolarisiertem Helium-3. *Fortschr Röntgenstr* (2000); **172**: 129–133.

Schuster D. The evaluation of lung function with PET. *Semin Nucl Med* (1998); **28**: 341–351.

Simon B, Marcucci C, Fung M, Lele S. Parameter estimation and confidence intervals for Xe-CT ventilation studies: a Monte Carlo approach. *J Appl Physiol* (1998); **84**: 709–716.

Snider GL, Kleinerman J, Thurlbeck WA, Bengali ZH. The definition of emphysema. *Am Rev Respir Dis* (1985); **132**: 182–185.

Verschakelen JA, Vanfraeyenhoven L, Laureys G, Demedts M, Baert AL. Differences in CT density between dependent and non-dependent portions of the lung: influence of lung volume. *AJR* (1993); **161**: 713–717.

White P, Hayward M, Cooper T. Ventilation agents - what agents are currently used? *Nucl Med Commun* (1991); **12**: 349–352.

Wild J, Schmiedeskamp J, Paley M *et al.* MR imaging of the lungs with hyperpolarized 3-Helium transported by air. *Phys Med Biol* (2002); **47**: N185–N190.

Yablonskiy D, Sukstanskii A, Leawoods J *et al.* Quantitative in vivo assessment of lung microstructure at the alveolar level with hyperpolarized $^{3}$He diffusion MRI. *Proc Natl Acad Sci USA* (2002); **99**: 3111–3116.